Initiation of Stress Corrosion Cracking for Pipeline Steels in a Carbonate-Bicarbonate Solution

Z.F. WANG and A. ATRENS

The linearly increasing stress test (LIST) was used to study the stress corrosion cracking (SCC) behavior of a range of pipeline steels in carbonate-bicarbonate solution under stress rate control at different applied potentials. Stress corrosion cracking, at potentials below −800 mV(SCE), was attributed to hydrogen embrittlement. Stress corrosion cracking, in the potential range from about −700 to −500 mV(SCE), was attributed to an anodic dissolution mechanism. In the anodic potential region, the SCC initiation stress was larger than the yield stress and was associated with significant plastic deformation at the cracking site. The relative SCC initiation resistance decreased with increasing yield strength. In the cathodic potential region, the SCC initiation stress was smaller than the yield stress of steel; it was approximately equal to the stress at 0.1 pct strain ($\sigma_{0.1\ pct}$) for all the steels. The original surface was more susceptible to SCC initiation than the polished surface.

I. INTRODUCTION

STRESS corrosion cracking (SCC) of steels in carbonate-bicarbonate solutions has been responsible for failures at a refinery catalytic cracking unit[1] and of natural gas pipelines.[2–6] Such service SCC occurs within a narrow potential region corresponding to the active to passive transition,[6–10] in which SCC is caused by anodic dissolution after strain breaks the corrosion product film on the specimen surface or at the crack tip. Less attention has been paid to SCC of pipeline steels at cathodic potentials, where SCC is caused by hydrogen embrittlement. Parkins[7] has shown that in service, the crack initiation process dominates the component lifetime because cracks propagate rapidly once initiated. However, a detailed study of SCC initiation is still lacking.

The linearly increasing stress test (LIST) is a new testing methodology developed by Atrens *et al.*[11] It is similar to the constant extension rate test (CERT) with the essential difference that LIST is load controlled, whereas CERT is displacement controlled. The LIST is a rapid method to evaluate SCC behavior, particularly to determine the SCC initiation stress.[11,12,13] The LIST technique has been used in the present research to study the SCC behavior of a range of pipeline steels in a carbonate-bicarbonate solution. The aim was to study the SCC susceptibility, especially to measure the SCC initiation stress, and to relate SCC behavior to the material properties, applied potential, stress rate, and surface condition.

II. EXPERIMENTAL PROCEDURE

The materials were commercial pipeline steels, X65(A), X65(B), X65(C), X52(A), X46(A), and X42(A), with chemical compositions and mechanical properties as shown in Tables 1 and 2.

Potentiodynamic polarization measurements were carried out at 20 °C, 50 °C, and 70 °C, in the absence of load, to evaluate the expected potential range for SCC using the methodology of Parkins.[14,15] The specimens were in the form of rods, 11.29 mm in diameter (*i.e.*, 1 cm² of surface area exposed to the solution). Before testing, the specimen surface was abraded with 800-grit silicon carbide paper. The potential was controlled with reference to a saturated calomel electrode (SCE) which was placed in a beaker containing the test solution at room temperature and was connected to the actual test solution through a Luggin probe. The specimen was held at −1300 mV(SCE) at room temperature for 5 minutes to remove surface oxide films, heated to the test temperature, and allowed 1 hour for stabilization. The polarization tests were started from the free corrosion potential, scanning in the anodic direction to 100 mV(SCE) at the rate of 10 mV/min and 1 V/min.

The SCC experiments were conducted in 1N Na_2CO_3 + 1N $NaHCO_3$ solution at 70 °C in a standard cell, as described previously,[11,12] using smooth tensile specimens (gage length = 10 mm, gage width = 3 mm, and gage thickness = 2.5 mm) with the original (*i.e.*, service) surface on one side and polished to 600-grit silicon carbide paper on the other side. To investigate the influence of polished *vs* original surface, some tests were carried out after masking off the polished surface or the original surface. The specimen length was parallel to the rolling direction with the result that the crack propagation direction was perpendicular to the actual cracking direction in service. However, it has been shown[16] that specimen orientation does not have a significant influence. Prior to testing, the specimen, except for the gage length, was coated with epoxy. The gage section was cleaned using alcohol and distilled water, and the specimen was loaded into the LIST apparatus immediately. Potential and temperature control were the same as that in the polarization tests.

The LIST test, described previously in detail,[11,12] allows application of a linearly increasing engineering stress to a specimen exposed to the environment of interest. This test is very similar to the CERT, except that CERT is controlled by the extension rate whereas LIST is controlled by the loading rate. The LIST apparatus (Figure 1) consists of a lever beam balanced at its equilibrium position. The loading

Z.F. WANG, Research Fellow, and A. ATRENS, Associate Professor, are with the Department of Mining and Metallurgical Engineering, The University of Queensland, Brisbane Qld 4072, Australia.

Manuscript submitted May 23, 1995.

Table I. Chemical Compositions of Steels (Wt Pct)

Steel	C	Mn	Si	S	P	Ni	Cr	Mo	Cu	V	Nb	Ti	Al
X65(A)	0.07	1.36	0.19	0.002	0.013	0.01	0.20	<0.01	0.01	<0.01	0.04	<0.01	0.011
X65(B)	0.055	1.40	0.25	0.005	0.016	0.01	0.25	<0.01	0.14	<0.01	0.03	<0.01	0.033
X65(C)	0.12	1.34	0.24	0.002	0.016	0.01	<0.01	<0.01	<0.01	<0.01	0.05	<0.01	0.030
X52(A)	0.16	1.32	0.31	0.006	0.017	0.01	0.01	<0.01	<0.01	<0.01	0.02	<0.01	0.030
X46(A)	0.10	0.60	0.13	0.014	0.016	0.01	<0.01	<0.01	<0.01	<0.01	0.02	<0.01	0.035
X42(A)	0.15	0.68	0.11	0.011	0.016	0.01	<0.01	<0.01	0.01	<0.01	<0.01	<0.01	0.035

Table II. Mechanical Properties of Steels

Steel	σ_y, MPa	σ_{UTS}, MPa	δ, Pct
X65(A)	446	560	31
X65(B)	490	545	23
X65(C)	470	570	29
X52(A)	434	580	32
X46(A)	426	500	31
X42(A)	420	486	29

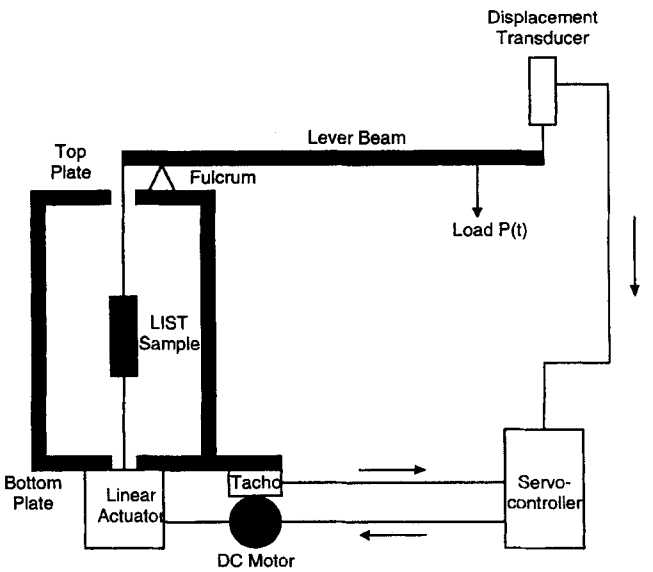

Fig. 1—Schematic drawing showing the principle of the LIST apparatus.[11,12] The load on the specimen is increased linearly by means of a lever principle and a linearly moving load on the right-hand side of the lever. The lever is maintained horizontal *via* a linear actuator and servocontroller by means of a displacement signal from the end of the lever arm.

train (including the test specimen) is connected to one side of the lever beam at a small, constant distance from the fulcrum. There is a known movable weight on the lever beam on the other side of the fulcrum. Movement of the weight along the lever beam away from the fulcrum, driven at a constant rate by a synchronous motor, causes a linearly increasing engineering stress to be applied to the specimen. By using synchronous motors of different speeds, various applied stress rates are achieved. The applied stress rates used in this study were 1.91×10^{-2}, 1.91×10^{-3}, and 1.91×10^{-4} MPa s^{-1}. A d.c. potential drop method was used to detect SCC initiation. A constant current of 5 A was applied to the specimen by means of two wires soldered onto the specimen ends, and the d.c. potential drop across the gage section was measured. In order to eliminate the influence of applied current fluctuation, a standard resistance was added to the measuring circuit. The measured parameter

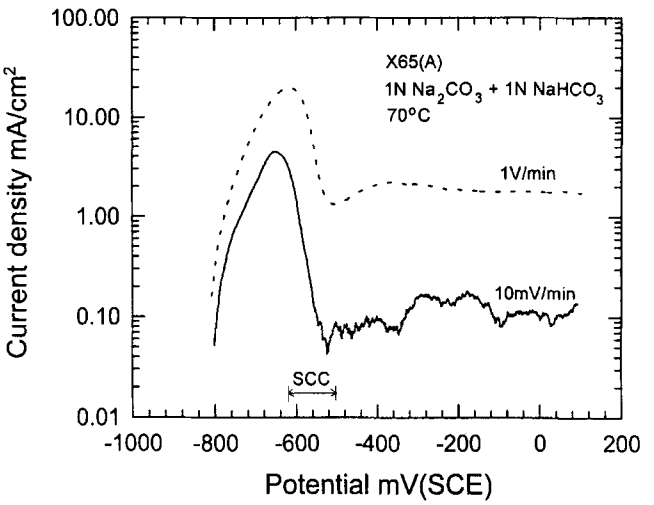

Fig. 2—Potentiodynamic polarization curves for X65(A) steel in carbonate-bicarbonate solution at 70 °C.

Table III. Potential Ranges for SCC (mV (SCE)) Predicted from the Potentiodynamic Polarization Curves According to References 14 and 15

	Potential Ranges for SCC (mV (SCE))		
Steel	20 °C	50 °C	70 °C
X65(A)	−600 to −480	−600 to −460	−620 to −500
X65(B)	−580 to −460	−640 to −520	−640 to −520
X65(C)	−560 to −450	−600 to −480	−640 to −540
X52(A)	−610 to −500	−620 to −520	−680 to −560
X46(A)	−560 to −440	−640 to −520	−640 to −520
X42(A)	−600 to −480	−620 to −520	−640 to −530

U/U_0 (U is a potential drop from the specimen gage section and U_0 is that from standard electric resistance) can reflect the deformation of the specimen and the SCC initiation processes. As shown in Section III, our present LIST experiments indicate that the onset of SCC is correlated with a significant change in slope of the curve of electrical resistance *vs* time in conformity with those reported in References 11 and 12.

III. RESULTS AND DISCUSSION

A. *Potentiodynamic Polarization Measurements*

Figure 2 gives a typical polarization curve for polished X65(A) steel at 70 °C. There was a well-defined active-passive transition at both scanning rates, with a higher current for the higher scanning rate. Table III gives the predicted potential ranges for SCC, evaluated according to the method in References 14 and 15, where there were large

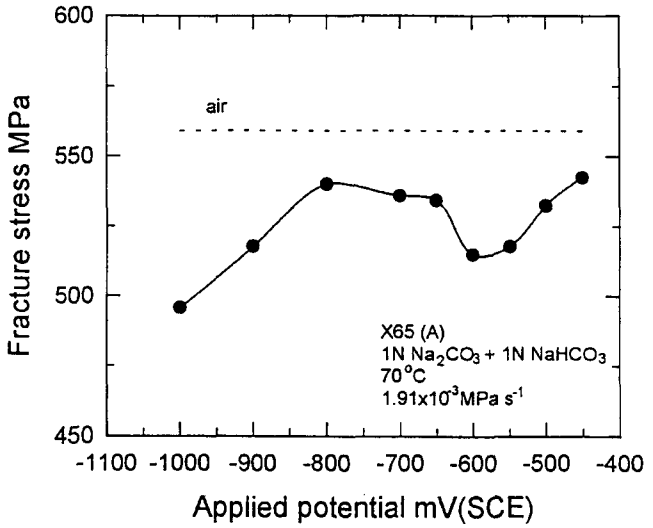

Fig. 3—Variation of fracture stress with applied potential for X65(A) steel in carbonate-bicarbonate solution at 70 °C.

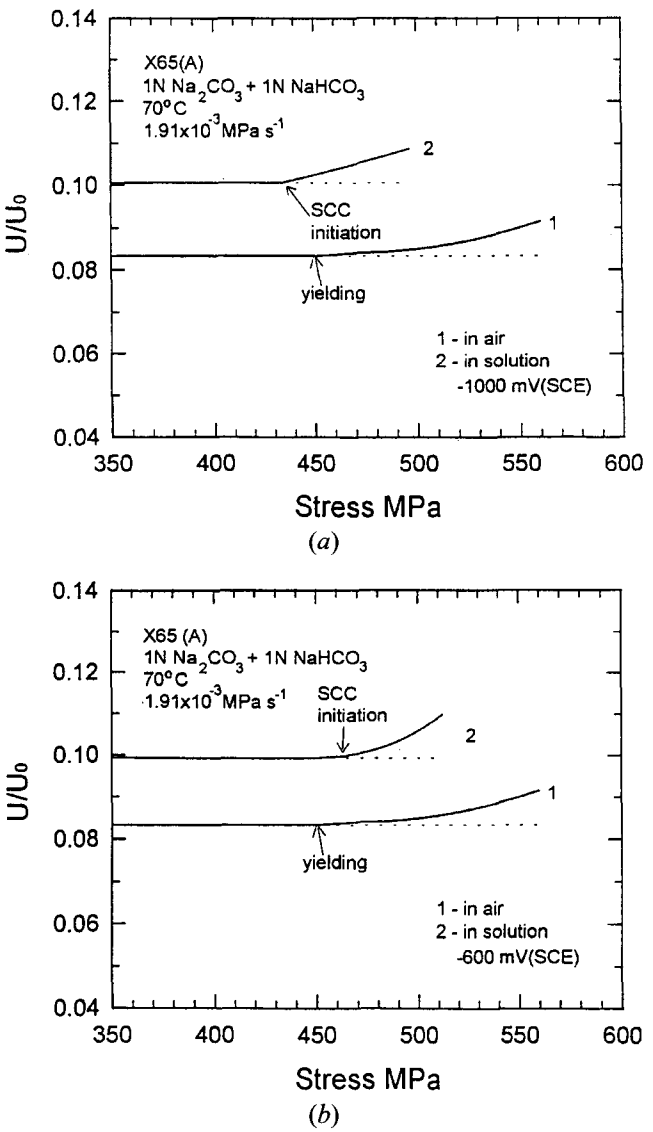

Fig. 4—Typical curves for the determination of the SCC initiation stress for X65(A) in carbonate-bicarbonate solution at 70 °C at (*a*) −1000 mV (SCE) and (*b*) −600 mV (SCE).

differences of current density between the two potentiodynamic curves. These results indicate that the predicted potential range was similar for all the alloys and moreover was similar at the three temperatures studied.

B. *Potential Dependence of SCC Susceptibility*

Figure 3 shows the variation with applied potential of the fracture stress for X65(A) at the applied stress rate of 1.91×10^{-3} MPa s^{-1}. The steel was susceptible to SCC within two potential regions, with the susceptibility greater at potentials below −800 mV(SCE) than at potentials from −700 to −500 mV(SCE). Within both regions, SCC cracks were easily observed on the specimen surfaces both by optical and scanning electron microscopy (SEM). In the cathodic potential region below −800 mV(SCE), SCC was visible by optical microscopy at low magnification; the number of cracks on the specimen surface increased with decreasing applied potential, and the crack size was much larger than at −600 mV(SCE). Within the anodic SCC potential range, the maximum SCC susceptibility, as measured by the minimum fracture stress, was at −600 mV(SCE).

The SCC is attributed to hydrogen embrittlement at potentials below −800 mV(SCE) and to anodic dissolution at potentials between −700 and −500 mV(SCE), with the experimental results showing that the pipeline steel is more susceptible to hydrogen embrittlement than to SCC caused by anodic dissolution at the same applied stress rate. In the anodic potential region, the LIST data indicated that the SCC potential range was from −700 to −500 mV(SCE), in good agreement with the expectations from the polarization curves. Therefore, the polarization curves do indeed predict the potential range for SCC for pipeline steels in carbonate-bicarbonate solutions.

C. *SCC Initiation*

The electrical resistance of the gage section increased during the tests due to the elastic and plastic elongation of the specimen. Once an SCC crack initiated, the resistance increased even further due to the reduction in cross-sectional area caused by the growing crack.

The SCC initiation stress could be determined from plots of U/U_0 against applied stress. Figure 4 shows typical curves of U/U_0 *vs* applied stress for X65(A) at the potential of (*a*) −1000 mV(SCE) and (*b*) −600 mV(SCE). When SCC initiates below the yield stress, then it is very easy to determine the SCC initiation stress; the U/U_0 curve increases rapidly at the SCC initiation stress before the yield stress is reached (*e.g.*, Figure 4(a)). Figure 4(b) shows that it is also possible to determine the SCC initiation stress when SCC initiates above the yield stress, because the increase in U/U_0 in the presence of SCC is significantly greater than the corresponding increase in air due to the onset of plastic deformation.

The SCC initiation stress for X65(A) steel at 70 °C, determined using this method (Figure 5), strongly depended upon the applied potential. Below the potential of about −925 mV(SCE), the SCC initiation stress was smaller than the yield stress and decreased with decreasing applied potential. In the anodic potential region, the SCC initiation stress was larger than the yield stress; the greatest suscep-

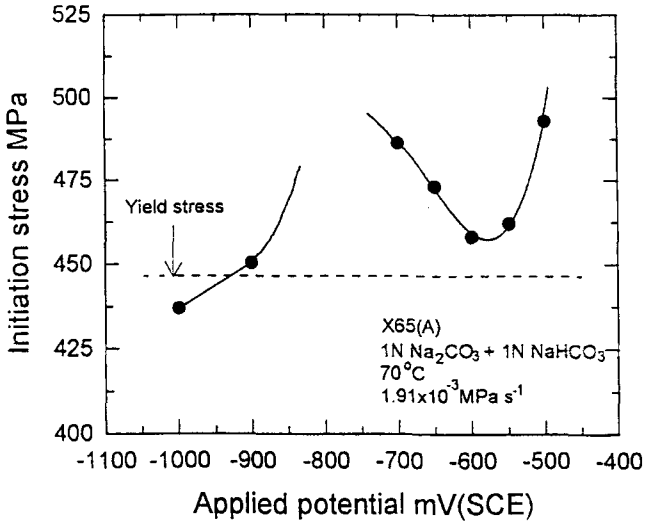

Fig. 5—Variation of the SCC initiation stress with applied potential for X65(A) in carbonate-bicarbonate solution at 70 °C.

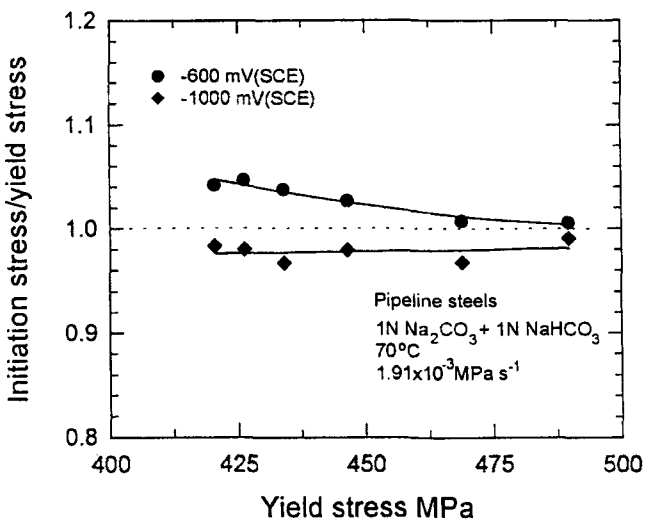

Fig. 6—Variation of SCC initiation stress/yield stress with the yield stress.

tibility was observed at −600 mV(SCE), in agreement with the maximum susceptibility as evaluated from the fracture stress (Figure 3). Between −900 and −700 mV(SCE), there was a higher resistance to SCC; the SCC initiation stress was large and difficult to determine.

The SCC initiation stresses for the other steels were determined; this led to Figures 6 and 7. Figure 6 shows the relationship between the SCC initiation stress/yield stress and the yield stress of commercial steels used for pipelines. At −600 mV(SCE), the SCC initiation stress was somewhat higher than the yield stress for lower yield strength steel and was approximately the same as the yield stress for higher yield strength steel. Thus, the relative SCC resistance under anodic dissolution control decreased with increasing yield strength, which was consistent with the literature results.[17,18,19] In contrast, at −1000 mV(SCE), the SCC initiation stress was below the yield stress and independent of yield strength; this was somewhat surprising in view of the expectation from the literature[20,21] of increasing susceptibility to hydrogen embrittlement with increasing strength.

Figure 7 plots the SCC initiation strain (determined from

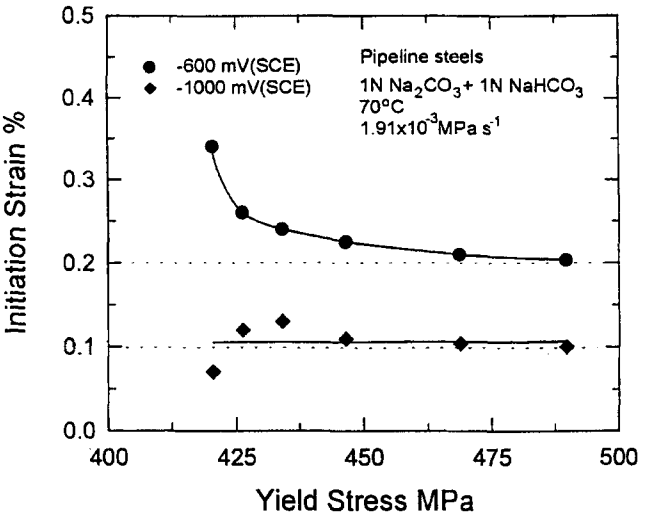

Fig. 7—Variation of the engineering strain at SCC initiation *vs* the yield strength.

the initiation stress and the stress-strain curves) *vs* the yield strength at −600 and −1000 mV(SCE) for commercial steels used for pipelines. At −600 mV(SCE), the SCC initiation strain was somewhat larger than the 0.2 pct yield strain and decreased with increasing yield strength to become approximately the same as the yield strain. At −1000 mV(SCE), the SCC initiation strain was nearly the same, equal to approximately 0.1 pct independent of the yield strength.

For SCC controlled by the anodic dissolution mechanism, it was reported[7] that the SCC initiation stress for pipeline steels in carbonate-bicarbonate solution was larger than the yield stress at a potential of −650 mV(SCE). This is consistent with the present results. Much experimental evidence has indicated that SCC is related to the plastic deformation process of the material;[22,23] SCC initiation can be discussed in terms of SCC initiating when the local plastic deformation at the cracking site reaches a critical value. For high strength steels, the critical plastic deformation can be reached locally before bulk yielding. In contrast, SCC initiation does not occur below the yield stress for very ductile low strength steels such as pipeline steels. The critical plastic deformation for crack initiation varies with the testing conditions, for example, material strength, potential, and applied stress rate, as shown in Figure 8. The SCC initiation stress decreased with decreasing applied stress rate. The SCC initiation stress was approximately equal to the yield stress for the test at the applied stress rate of 1.91×10^{-4} MPa s^{-1}. For SCC controlled by anodic dissolution, passivation competes with the depassivation caused by strain breaking the crack-tip film. There is competition between the corrosion processes and the applied stresses. At higher strain rates, ductile failure occurs because there is insufficient time for the corrosion processes. At lower applied stress rates, repassivation becomes increasingly important; Figure 8 is in this regime.

For SCC controlled by hydrogen embrittlement, SCC initiation depends on the entrance of hydrogen into the specimen at the cracking site. Hydrogen-induced cracking occurs when a critical hydrogen concentration is reached at the cracking site. There does not seem to be any requirement for a relation between the crack initiation stress and

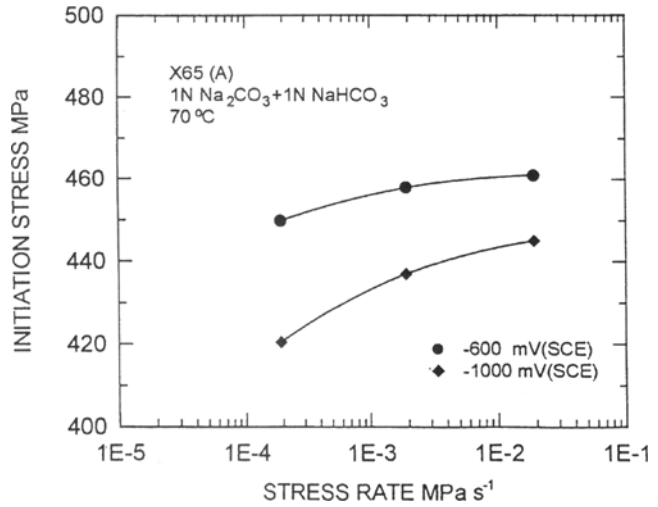

Fig. 8—Effect of applied stress rate on the SCC initiation stress for X65(A).

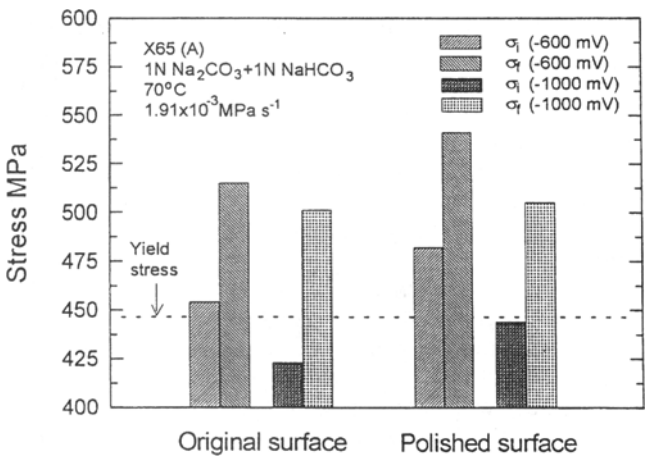

Fig. 9—Effect of specimen surface condition on the fracture and initiation stresses.

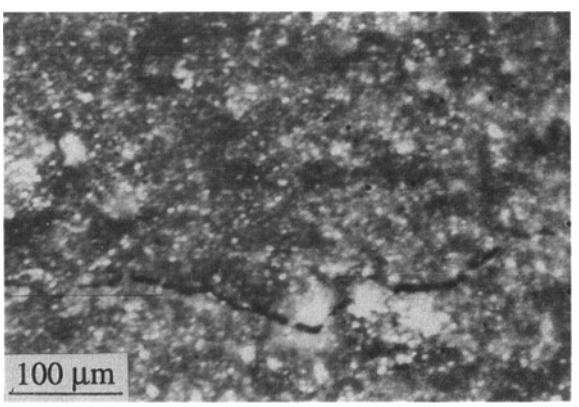

Fig. 10—Breaking of the original surface film at applied stress of 430 MPa during elongation of the specimen in air.

yield stress in this case. However, there should be a critical stress for SCC, and hydrogen-induced cracking does not happen below this stress even if the critical hydrogen concentration is reached. Wang *et al.*[24] has shown that, for low strength material, the diffusion of hydrogen into the matrix is not the controlling step and that mechanical parameters play a dominant role during cracking. In the present tests, this mechanical parameter can be identified as either a critical stress (0.98 σ_y) or a critical strain (0.1 pct). As for the SCC under the control of the anodic dissolution mechanism, SCC initiation under control of hydrogen embrittlement was dependent on applied potential and the applied stress rate. At a more negative potential, the amount of hydrogen absorbed by the steel is larger, leading to a decrease in the SCC initiation stress. Figure 8 shows that the SCC initiation stress decreased with decreasing applied stress rate. A lower stress rate allows more time for the entrance of hydrogen into the specimen matrix resulting in the decrease of the SCC initiation stress.

D. *Effect of Specimen Surface Conditions and Possible SCC Initiation Mechanism*

Each specimen had an original surface on one side and a polished surface on the other side. The influence of the original surface on the SCC behavior for X65(A) steel in carbonate-bicarbonate solution at 70 °C was studied by using specimens coated on one specimen side with silastic which cannot be broken during specimen deformation. The results (Figure 9) indicated that the original surface was much more susceptible to SCC initiation than the polished surface for SCC controlled both by anodic dissolution and hydrogen embrittlement. The original surface is covered with an oxide/corrosion-product film produced during pipe manufacturing; this film is brittle and breaks during the elongation of the specimen. Figure 10 shows the appearance of the original surface at an applied stress of 430 MPa for X65(A) steel in air. The original surface film cracked at this applied stress. The cracks became larger and new cracks initiated with increasing applied stress. It is interesting that the stress for cracking the original surface film in air is just below the yield stress of the steel and is located between the SCC initiation stress under anodic dissolution control and that under hydrogen embrittlement control.

For SCC controlled by the anodic dissolution mechanism, the original surface film broke below the yield stress and this was associated with a lower SCC initiation stress. As these experiments were carried out at controlled potentials in the middle of the cracking range, there would be a high local current density at rupture sites in the original film which would promote local plasticity and thereby facilitate crack initiation at lower stresses. This is similar to the work of Jones,[23] who indicated that for a freely corroding specimen, an exposed bare surface at a rupture site had a transient potential that was considerably more active than the passive surface potential. However, such a bare surface was anodically polarized to the passive potential by its coupling to the relatively large surrounding passive surfaces. As a result, the local anodic current density would be very high because of the high ratio of anode to cathode surface area. This would promote localized plasticity by attenuation of strain hardening at the rupture sites. This localized plasticity allowed earlier SCC crack initiation when the required local minimum plastic deformation was reached, *i.e.*, decreased the SCC initiation stress. It has also been reported that a specimen with the coarsest grit finish had a strain for SCC initiation lower than that for a specimen with a fine grit finish.[25] The rougher surface was associated with a greater local stress concentration, there-

fore, greater local plasticity and consequently higher SCC initiation susceptibility.

For SCC controlled by hydrogen embrittlement, however, there seems to be little relation between the SCC initiation and the breaking of the original surface film, because the SCC initiation stress is slightly lower than the stress for breaking the original surface film. It is concluded that the breaking of the original surface film is not the cause of SCC initiation. The hydrogen must be able to enter the metal through the original surface film. The SCC initiation occurs simply due to a critical hydrogen concentration in the specimen matrix combined with the applied tensile stress; *i.e.*, a critical stress intensity is reached at local sites on the specimen surface at a critical flaw. The original surface is more susceptible to SCC initiation, probably because there are concentrations of stress and chemical composition of aggressive species on the original specimen surface.

IV. CONCLUSIONS

1. The SCC tests confirmed the potential range for SCC predicted by the polarization tests. The susceptible potential ranges for SCC for pipeline steels in the carbonate-bicarbonate solution at 20 °C, 50 °C and 70 °C are shown in Table III for SCC controlled by anodic dissolution. However, the steel was more susceptible to hydrogen embrittlement than anodic dissolution at the same applied stress rate.
2. For SCC controlled by anodic dissolution, the SCC initiation stress was larger than the yield stress of steel. The relative SCC initiation resistance decreased as the yield strength of the steel was increased.
3. For SCC controlled by hydrogen embrittlement, the SCC initiation stress was lower than the yield stress of the steel. There was approximately the same SCC initiation susceptibility for all the commercial steels examined. The SCC initiation stress for each steel was close to $\sigma_{0.1}$ pct.
4. The original surface was more susceptible to SCC initiation than the polished surface. At anodic potentials, the original surface film broke before SCC cracking initiated. This breaking of the original surface film accelerated the SCC initiation process. At cathodic potentials, SCC cracking initiated before the original surface film broke. Stress corrosion cracking initiation had little relation to the breaking of original surface film.

ACKNOWLEDGMENTS

This work was supported by East Australia Pipeline Ltd.

REFERENCES

1. J.H. Kmetz and D.J. Truax: *Corrosion 90*, NACE, Houston, TX, 1990, paper no. 206.
2. J.P. O'Donnell: *Oil Gas J.*, 1970, vol. 69 pp. 77-79.
3. H.E. Townsend: *Mater. Protect. Performance*, 1972, vol. 11, pp. 33-37.
4. P.J. Kentish: *Br. Corros. J.*, 1985, vol. 20, pp. 139-46.
5. G.J. Ogundele and R.D. Venter: *Corrosion 89*, NACE, Houston, TX, 1989, paper no. 572.
6. R.N. Parkins: *5th Symp. on Line Pipe Research*, American Gas Association Inc., Houston, TX, 1974, paper no. V.
7. R.N. Parkins, E. Belhimer, and W.K. Blanchard: *Corrosion*, 1993, vol. 49, pp. 951-66.
8. R.N. Parkins, P.W. Slattery, and B.S. Poulson: *Corrosion*, 1981, vol. 37, pp. 650-64.
9. R.N. Parkins: *EICM Proc.*, p. 1.
10. J.M. Sutcliffe, R.R. Fessler, W.K. Boyd, and R.N. Parkins: *Corrosion*, 1972, vol. 28, pp. 313-20.
11. A. Atrens, C.C. Brosnan, S. Ramamurthy, A. Ochlert, and I.O. Smith: *Meas. Sci. Technol.*, 1993, vol. 4, pp. 1281-92.
12. S. Ramamurthy and A. Atrens: *Corros. Sci.*, 1993, vol. 34, pp. 1385-1402.
13. J. Salmond and A. Atrens: *Scripta Metall.*, 1992, vol. 26, pp. 1447-50.
14. R.N. Parkins: *Corros. Sci.*, 1980, vol. 20, pp. 147-66.
15. N.J.H. Holroyd and R.N. Parkins: *Corros. Sci.*, 1980, vol. 20, pp. 707-21.
16. J.A. Beavers, W.E. Berry, and R.N. Parkins: *Mater. Performance*, 1986, vol. 25 (6), pp. 9-17.
17. E.H. Phelps: *Proc. Conf. Fundamental Aspects of Stress Corrosion Cracking*, Ohio State University, Columbus, OH, 1967.
18. A.W. Coulter and T.S. Claiborne: *Mater. Protect.*, 1968, vol. 7 (6), pp. 23-26.
19. R.D. McDonald: *Weld. Res. Abroad*, 1972, June, pp. 23-26.
20. E. Snape: *Corrosion*, 1967, vol. 23, pp. 154-72.
21. J.E. Campbell: DMIC Report No. S-31, Apr. 1970.
22. R.N. Parkins: *JOM*, 1992, Dec., pp. 12-19.
23. D.A. Jones: *NACE 10—Environment-Induced Cracking of Metals*, R.P. Gangloff and M.B. Ives, eds., NACE, Houston, TX, 1990, pp. 265-70.
24. Z.F. Wang, J. Li, J.Q. Wang, and W. Ke: *Corros. Sci.*, 1995, vol. 37, pp. 1551-65.
25. W. Yang, J. Congleton, O. Kohneh-Chari, and P. Sajdl: *Corros. Sci.*, 1992, vol. 33, pp. 735-50.